JCTC Journal of Chemical Theory and Computation

Article

pubs.acs.org/JCTC

Understanding the Electronic Factors Responsible for Ligand Spin−Orbit NMR Shielding in Transition-Metal Complexes

Jan Vícha,[†] Cina Foroutan-Nejad,[†,‡] Tomasz Pawlak,[†,⊥] Markéta L. Munzarová,[†,§] Michal Straka,*[,†,∥] and Radek Marek*[,†,§]

[†]CEITEC—Central European Institute of Technology, Masaryk University, Kamenice 5/A4, CZ-62500 Brno, Czech Republic

[‡]National Center for Biomolecular Research, Faculty of Science, Masaryk University, Kamenice 5, CZ-62500 Brno, Czech Republic

[§]Department of Chemistry, Faculty of Science, Masaryk University, Kamenice 5, CZ-62500 Brno, Czech Republic

[∥]Institute of Organic Chemistry and Biochemistry of the ASCR, Flemingovo nám. 2, CZ-16610, Praha, Czech Republic

Supporting Information

ABSTRACT: The significant role of relativistic effects in altering the NMR chemical shifts of light nuclei in heavy-element compounds has been recognized for a long time; however, full understanding of this phenomenon in relation to the electronic structure has not been achieved. In this study, the recently observed qualitative differences between the platinum and gold compounds in the magnitude and the sign of spin−orbit-induced (SO) nuclear magnetic shielding at the vicinal light atom (^{13}C, ^{15}N), σ^{SO}(LA), are explained by the contractions of 6s and 6p atomic orbitals in Au complexes, originating in the larger Au nuclear charge and stronger scalar relativistic effects in gold complexes. This leads to the chemical activation of metal 6s and 6p atomic orbitals in Au complexes and their larger participation in bonding with the ligand, which modulates the propagation of metal-induced SO effects on the NMR signal of the LA via the Spin−Orbit/Fermi Contact (SO/FC) mechanism. The magnitude of the σ^{SO}(LA) in these square-planar complexes can be understood on the basis of a balance between various metal-based 5d → 5d* and 6p → 6p* orbital magnetic couplings. The large and positive σ^{SO}(LA) in platinum complexes is dominated by the shielding platinum-based 5d → 5d* magnetic couplings, whereas small or negative σ^{SO}(LA) in gold complexes is related to the deshielding contribution of the gold-based 6p → 6p* magnetic couplings. Further, it is demonstrated that σ^{SO}(LA) correlates quantitatively with the extent of M−LA electron sharing that is the covalence of the M−LA bond (characterized by the QTAIM delocalization index, DI). The present findings will contribute to further understanding of the origin and propagation of the relativistic effects influencing the experimental NMR parameters in heavy-element systems.

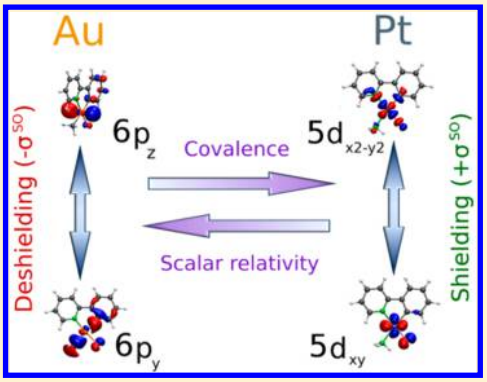

1. INTRODUCTION

The effects of relativity on the electronic structure and properties of molecules have been widely explored since the early 1970s when the full relevance of relativistic effects in heavy-element chemistry was discovered.[1,2] The yellow color of gold and cesium, the unusually low boiling point of mercury, or the stability of low oxidation states of Tl^{I}, Pb^{II}, and Bi^{III} are just a few examples of how relativity manifests itself in the observable world.[3]

Somewhat less known but equally interesting are the relativistic effects on the parameters of nuclear magnetic resonance (NMR).[4] In the HALA effect (Heavy Atom on the Light Atom), the heavy atom (HA) in a molecule induces relativistic shielding or deshielding at the light NMR nuclei (LA) nearby. The Heavy Atom on Heavy Atom itself (HAHA) effect is important for the NMR of heavy nuclei, such as ^{195}Pt and ^{199}Hg.[5] The HAVHA (Heavy Atom on Vicinal Heavy Atom) was coined recently for compounds containing more relativistic centers,[6] such as HXeI.[7] The knowledge on relativistic effects in NMR was summarized in several review articles, e.g., refs 5, 8, and 9.

The HALA effect in chemical compounds is typically dominated by the spin−orbit coupling at the heavy atom (SO-HALA effect)[5] propagated mainly via the dominant SO/FC (Spin−Orbit/Fermi-Contact) mechanism. The SO/FC mechanism was suggested already in the 1960s[10−12] and has been subsequently discussed in numerous studies.[6,13−21] For a systematic account of different contributions to the HA−LA chemical shift, see studies by Nakatsuji et al.,[22,23] Vaara et al.,[24−27] and Aucar et al.[6,28−32] This third-order property is given schematically as[25,33,34]

$$\sigma_{N,uv}^{SO/FC} = \frac{\partial^2}{\partial\mu_{N,u}\partial B_{0,v}}\left[\sum_{m,n\neq 0}\frac{\langle 0|H_{N,u}^{FC}|m\rangle\langle m|H^{SO}|n\rangle\langle n|H_{v}^{OZ}|0\rangle}{(E_0-E_m)(E_0-E_n)} + \text{permutations}\right] \quad (1)$$

Received: December 3, 2014
Published: March 4, 2015

DOI: 10.1021/ct501089z
J. Chem. Theory Comput. 2015, 11, 1509−1517

Here, μ denotes the nuclear magnetic moment and B_0 the external magnetic field. The total energies E in the denominator pertain to excited states of the system,[33] and the double sum runs over all excited states. $\mathbf{H}^{FC}$ in the first matrix element denotes the hyperfine operator. The second and third matrix elements account for the SO operator and for the orbital Zeeman interaction with the external magnetic field, respectively.

The understanding of how HALA effects reflect the electronic structure and bonding in the heavy-atom molecules has been a subject of interest since the early studies. For reviews, see refs 5 and 8. In 1987, Pyykko and Görling pointed out that in the HI molecule the σ-type orbitals give rise to a deshielding effect at the hydrogen atom, whereas π-type orbitals give rise to a shielding effect.[14] This is related to the previous rationalizations of ^{195}Pt and ^{31}P NMR chemical shifts using similar σ/π arguments and covalence of ligand bonding reported in the late 1960s.[35,36] In 1998, Wolf and Ziegler further demonstrated that for the 5d transition-metal complexes, the balance between the σ- and π-type HA−LA bonding relates to the size of the σ^{SO} contribution to the LA NMR shielding constant.[37] In the same year, Kaupp et al. noted that the σ^{SO}(LA) is proportional to the s character of the LA atom in the HA−LA bond in a series of halogenated hydrocarbons and pointed out the resemblance of the SO/FC HALA mechanism with that of indirect nuclear spin−spin coupling.[17] The analogy was demonstrated by the Karplus-like dependence of σ^{SO} on the dihedral angle for LA three bonds away from the HA. The role of the ligand field affecting the $\sigma^{SO}(^1H)$ shielding in the chelates of cobalt-group-metal centers via the energy denominators (eq 1) and the effect of the *trans* ligand were discussed by Hegetschweiler et al. in 2004 and Hyvärinen et al. in 2009.[13,38] The relationship between the magnitude of the σ^{SO} effect and the covalence/ionicity of the HA−LA bond was indicated in studies by Pawlak et al.[39] and Truflandier et al. in 2011.[40,41]

Recently, we have demonstrated that in octahedral Ir^{III} as well as square-planar Pt^{II} complexes, the σ^{SO}(LA) at the light atom of the ligand (LA) directly bonded to the metal center (M) sensitively reflects changes of the substituent *trans* to the LAs.[42,43] A closer analysis revealed that the s character of LA in the M−LA bond was almost intact, while the metal d character of the M−LA bond was strongly modulated by the *trans* ligand.[43] This led to the concept of "bonding d character", i.e., correlation of σ^{SO}(LA) with a metal d-orbital character of the M−LA bond.

The present study was motivated by our observation of rather striking differences in the σ^{SO} at ligand atoms bonded to the heavy-metal center in the square-planar Pt and Au complexes with 2-phenylpyridine,[39] similar to those listed in Figure 1. We found that the σ^{SO} contribution to the nuclear shielding of N1 and C2′ ligand atoms bound directly to the central metal atom is rather large and positive (shielding) in the Pt complexes but small or even negative (deshielding) in the Au complexes.

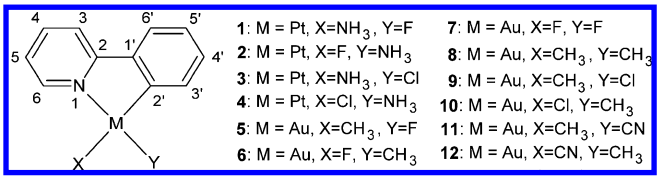

Figure 1. Structure and atom numbering scheme for complexes **1**−**12**.

To investigate the nature of the large differences in σ^{SO}(LA) among the Au and Pt complexes, we studied a series of compounds shown in Figure 1. These species are typical d^8 square-planar complexes with metal 5d orbitals split by a crystal field as schematically outlined in Figure 2. The 5d orbitals located in the "ligand" plane are highly destabilized (especially the formally vacant $5d_{x^2-y^2}$), whereas out-of-plane orbitals lie significantly lower in the energy. In real complexes, orbital energy levels in this schematic picture are further split by the lower symmetry of the ligand field as well as by spin−orbit coupling effects, *vide infra*.

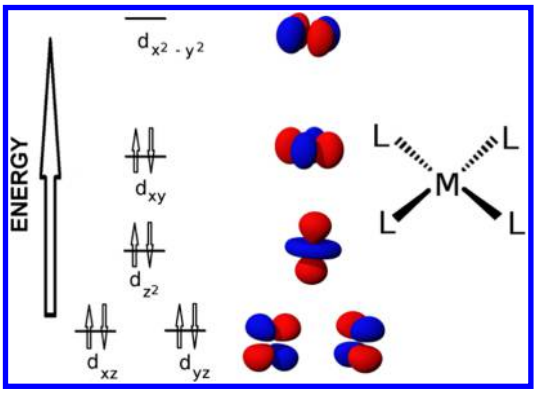

Figure 2. Schematic energy levels of valence atomic d orbitals of transition metal in the d^8 electron configuration and square-planar arrangement of the crystal field.

In this work, we search for a detailed understanding of the SO/FC HALA mechanism of nuclear magnetic shielding at LA, σ^{SO}(LA), in the square-planar Pt and Au complexes. We analyze the influence of the central metal atom, the type of ligand, particularly in connection with *trans* effect, and the degree of covalence of the metal−ligand (M−LA) bonds on the σ^{SO}(LA). We investigate how the magnitude and sign of the σ^{SO}(LA) reflect the electronic structure of Au^{III} and Pt^{II} complexes.

The SO-induced nuclear magnetic shielding is calculated and analyzed for a series of compounds shown in Figure 1. The SO/FC contribution in eq S1 is correlated with different chemical bonding schemes, such as MO, NBO, or QTAIM, to reveal the relationship between the σ^{SO}(LA) and electronic structure of the complex, particularly the nature of the M−LA bond. We show that different SO effects on σ^{SO}(LA) in Au and Pt complexes can be traced to different orbitals involved in the metal−ligand bonding. Notable correlation between the magnitude of SO-induced shielding at the light atom and covalence of metal−ligand bond is demonstrated.

2. COMPUTATIONAL DETAILS

Molecular Structures. 2-Phenylpyridine (2ppy), which is known to bind well both Pt^{2+} and Au^{3+} ions,[44−47] was selected as a chelating ligand for the series of model compounds, **1**−**12**, listed in Figure 1. The structures of the d^8 square-planar complexes **1**−**12** were minimized *in vacuo* using the PBE0[48] functional and the def2-TZVPP basis sets for light atoms[49] as implemented in the Turbomole 6.3.1 code.[50] The effective-core potentials (ECPs)[51] substituting 60 electrons in the core region (ECP-MDF-60) were used for the heavy Pt and Au atoms together with corresponding basis sets of def2-TZVPP quality for explicit valence electrons (18-VE for Pt and 19-VE for gold).[49] This computational level was justified in previous methodological studies of transition-metal complexes and is referred to as PBE0/def2-TZVPP in the present study.[42,45,52]

DOI: 10.1021/ct501089z
J. Chem. Theory Comput. 2015, 11, 1509−1517

Analysis of Electronic Structure. The composition of molecular orbitals (MOs) was determined as the net Mulliken population using the Gaussian 09 (G09) program. Natural Bond Orbital (NBO) analysis[53] as implemented in the NBO 5.9 module (Gennbo)[54] interfaced to ADF code, release 2013,[55] was performed.

Quantum Theory of Atoms in Molecules. QTAIM analysis was performed using the PBE[56,57] functional, def2-SVP basis set for light atoms,[49] and ECP-MWB-60 with def2-TZVPP for gold and platinum.[49,51] Auxiliary s-type core electron functions were added manually to the molecular wave functions to model the ECP core electrons of Au and Pt atoms.[58−60] The auxiliary wave function does not contribute in the Atoms in Molecules properties; i.e., it has no effect on the charge- or energy-related properties and does not change the magnitude of delocalization index—a property we are employing in the present work. Nevertheless, auxiliary wave functions are necessary to prevent the appearance of spurious critical points around nuclei, where core electrons are absent in the ECP approach. This in fact allows for integrating over the atomic basins and provides a route toward computation of the basin properties. Wave function was analyzed, and the delocalization index between all pairs of atoms was computed using the AIMAll suite of programs.[61] Delocalization index, DI or δ(M↔LA), measures the magnitude of electron sharing between two atomic basins and is a direct measure of covalence.[62,63]

Calculation and Analysis of σ^{SO}. Calculations and MO analyses of σ^{SO} were performed in the MAG 2.1 suite[64,65] interfaced with Gaussian 09 (G09).[66] Calculations of σ^{SO} used sum-over-state finite-field third-order perturbation theory (SOS-DFPT, see eq S1)[67,68] with the finite Fermi-contact perturbation set equal to 0.001 au on either N1 or C2′ nuclei. The calculations were done with the PBE[56,57] functional and def2-SVP basis set for the light atoms.[50] For heavy atoms, Pt and Au, the scalar-relativistic effective core potentials (ECPs) with 60 electrons in the core (ECP-MWB-60) together with def2-TZVP basis sets as defined in the Turbomole code were used.[50,51,66] The shielding calculations in MAG used corresponding spin−orbit SO-ECPs.[51,66] This level is referred to as PBE/def2-TZVP/def2-SVP in this work (for an analogous study, see ref 43).

The results obtained with the MAG 2.1 suite[64,65] were compared with those calculated by using the ADF2013 code,[55] where the σ^{SO} was calculated using the two-component zeroth-order regular approximation (SO-ZORA) approach.[69,70] The hybrid functional based on PBE0 with 40% of exact-exchange admixture (PBE-40) and the TZP basis set were used based on their good performance for calculations of NMR parameters revealed in our study of octahedral Ir^{III} and Pt^{IV} complexes.[42] The corresponding levels are referred to as PBE-40/TZP/SO-ZORA and PBE-40/TZP/ZORA in calculations with and without (for NBO analysis) the SO operator, respectively.

3. RESULTS AND DISCUSSION

The calculated σ^{SO}(N1) and σ^{SO}(C2′) are analyzed and discussed for selected complexes **1** and **2** (Pt) and **5** and **6** (Au), shown in Figure 3. Detailed results for all species **1**−**12** shown in Figure 1 are given in the Supporting Information, Tables S1−S8. The σ^{SO} values for N1 and C2′ atoms in **1** and **2** and **5** and **6** are listed in Table 1. The σ^{SO}(LA) in gold compounds **5** and **6** is significantly reduced in size for both N1 and C2′ and even negative in some cases, as anticipated above.[39]

MAG code has been used to analyze contributions of individual MO → MO* magnetic couplings to the σ^{SO}(LA), where MO refers to an occupied molecular orbital and MO* to a virtual molecular orbital (typically metal-centered orbitals). Because the appropriate tools needed for MO analysis of σ^{SO}(LA) are currently available only at the GGA DFT level (here PBE), the SO-ZORA calculations at the PBE-40/TZP level were performed as a reference[42] to check the quality of the MAG data. The results are given in Table 1. The MAG data somewhat deviate from the SO-ZORA values (mainly due to the missing exact-exchange in the PBE functional and, to a small extent, also due to the higher-order relativistic effects included in the latter), but the overall trends are clearly preserved. This allows us to analyze the individual MO → MO* contributions to the σ^{SO}(LA) while maintaining reasonable accuracy to describe and understand the general trends in σ^{SO}(LA) of the studied complexes, *vide infra*.

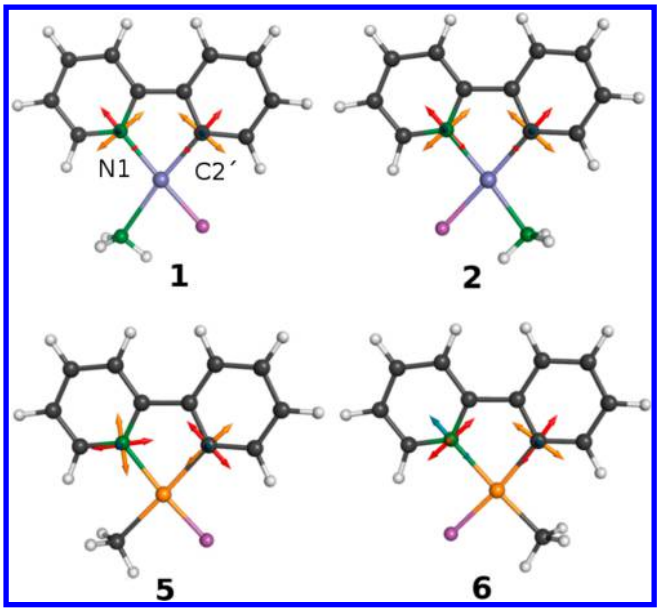

Figure 3. Structures of complexes **1** and **2** (Pt) and **5** and **6** (Au) calculated at the PBE0/def2-TZVPP level along with the orientations of σ^{SO}_{xx} (red), σ^{SO}_{yy} (orange), and σ^{SO}_{zz} (blue) principal axes of N1 and C2′ spin−orbit (SO) shielding tensors discussed in section 3.2

Table 1. Calculated σ^{SO}(N1) and σ^{SO}(C2′), the s Character of LA and the d Character of M in the M−LA Bond for Compounds 1, 2, 5, and 6 [σ^{SO}(LA) in ppm, s and d Character in %]

N1	1	2	5	6
σ^{SO} MAG[a]	34.1	28.2	10.6	−17.8
σ^{SO} ADF[b]	42.2	30.1	20.7	−15.3
s character LA[c]	29	28	27	26
d character M[c]	56	54	56	48
C2′	**1**	**2**	**5**	**6**
σ^{SO} MAG[a]	37.0	42.5	−5.5	20.9
σ^{SO} ADF[b]	31.5	35.0	−8.0	18.9
s character LA[c]	28	29	26	27
d character M[c]	52	54	49	57

[a]PBE/def2-TZVP/def2-SVP. [b]PBE-40/TZP/SO-ZORA. [c]PBE-40/TZP/ZORA; see Computational Details section for details.

3.1. Analysis of the Light Atom s-character and Metal Atom d-character of the M−LA Bonds in Pt^{II} and Au^{III} Complexes.

As discussed in the Introduction, the σ^{SO}(LA) has previously been found to correlate with the light-atom s character or with the metal d character of the M−LA bond. Therefore,

DOI: 10.1021/ct501089z
J. Chem. Theory Comput. 2015, 11, 1509−1517

these parameters are summarized in Table 1. We note that the differences in the light-atom s character in the M−LA bond for **1** vs **5** and **2** vs **6** compounds are rather small, about 2%. This tiny change may influence the σ^{SO}(LA), but by itself it rationalizes neither the differences of more than 40 ppm for σ^{SO}(N1) between the platinum and gold compounds (**2** vs **6**) nor the changes in the sign of σ^{SO}(LA) (positive/negative, Table 1). This is in line with our recent observation[43] of the lack of correlation between the σ^{SO}(LA) and the nitrogen s character of the Ir−N bond in octahedral complexes of Ir^{III}. We note, however, that despite no quantitative correlation of the σ^{SO}(LA) with the LA s character, as seen in Tables 1 and S1, the s character of LA is an essential factor for the SO/FC mechanism to take place.[17] The M−N1 and M−C2′ bonds *do have* a substantial LA 2s character, but it remains almost constant upon varying the substituents or changing the central metal atom (see Table 1).

We have recently demonstrated for octahedral Ir^{III} and square-planar Pt^{II} complexes that the σ^{SO}(LA) correlates well with the metal d character of the M−LA bond (bonding d character concept, BDC).[43] Examples of BDC correlation of σ^{SO}(N1) and σ^{SO}(C2′) with metal d character of M−N1 and M−C2′ bonds for Au(III) complexes **5**−**12** studied here are shown in Figures S1 and S2. These dependencies extend further the validity of the BDC concept beyond the platinum and iridium complexes toward the square-planar complexes of gold. However, it cannot be utilized as a relevant descriptor to understand the differences between Au and Pt complexes in this study, because the concept works only for series of compounds with a given central metal atom. Hence, the full MO analysis of σ^{SO} was performed to unveil the striking differences in the σ^{SO}(LA) between Pt and Au species.

3.2. MO Analysis of σ^{SO}(LA): Electronic Structure Motifs Altering the Sign of the σ^{SO}(LA). The SOS-DFPT approach to the SO/FC mechanism used in this study (eq S1 in Supporting Information) allows for the MO analysis of σ^{SO}(LA) in which the total σ^{SO}(LA) can be factorized in the contributions from individual occupied → virtual (MO → MO*) orbital magnetic couplings.[68] The main trends in σ^{SO} along a series of molecules can be typically traced to a few MO → MO* magnetic couplings, which thus provide a correlation between the electronic structure and σ^{SO}. The "σ^{SO}-active" occupied MOs[43] can be identified as MOs, which, within some threshold (in the present case >2.5 ppm), contribute to the particular σ^{SO}(LA). For the complexes **1**−**12** studied here, the σ^{SO}-active MOs could be easily identified and analyzed in terms of the energy and composition; see Table 2 for compounds **1**−**2** and **5**−**6** and Table S2 for compounds **3**−**4** and **7**−**12**.

An important connection to make here is the observation that σ^{SO}-active MOs responsible for the negative σ^{SO} contribution in compounds **1**−**12** are typically of σ symmetry with respect to the M−LA bond (*vide infra*), while those with the positive contributions are of π symmetry with respect to the M−LA bond.[14] The relation between σ/π symmetry and the negative/positive sign of the σ^{SO}(LA) confirms previous findings and opens the question of how is the positive or negative sign of σ^{SO}(LA) related to orbitals involved in M−LA bonding.[8,14,37]

In Pt complexes, where the σ^{SO} is typically large and positive (see Table 1), the corresponding σ^{SO}-active MOs have substantial Pt 5d character and marginal or no Pt 6s or 6p character (see Table 2). In contrast, in Au complexes, where the σ^{SO}(LA) is typically small or even negative (see Table 1), the σ^{SO}-active MOs, especially those with negative contribution to σ^{SO}(LA) have typically appreciable Au 6s and/or 6p character (see Table 2). This is probably one of the most important observations made

Table 2. Calculated[a] Total σ^{SO}(LA) for LA = N1 and C2′; the Contributions of σ^{SO}-Active MOs to Total σ^{SO}(LA), σ^{SO}(MO), and MO Energies (E^{MO}); and Contributions of Metal AOs to the Particular MO for 1and 2 and for 5 and 6 (NMR Shielding Constants in ppm, Energies in a.u., and AO Contributions in %)

compound	σ^{SO}(N1)	MO	σ^{SO}(MO)	E^{MO}	relative contribution of metal AO to MO		
					5d	6s	6p
1	34.1	56	11.9	−0.192	98	2	0
		59	26.0	−0.171	98	0	2
2	28.2	56	25.2	−0.199	100	0	0
5	10.6	52	3.2	−0.290	100	0	0
		55	3.1	−0.241	88	0	12
		58	3.1	−0.220	100	0	0
6	−17.8	54	−12.5	−0.256	39	50	11
		55	−8.4	−0.248	60	25	15
compound	σ^{SO}(C2′)	MO	σ^{SO}(MO)	E^{MO}	relative contribution of metal AO to MO		
					5d	6s	6p
1	37	56	22.0	−0.192	98	2	0
		58	12.9	−0.181	100	0	0
2	42.5	57	19.3	−0.193	96	4	0
		59	19.5	−0.162	100	0	0
5	−5.5	43	9.7	−0.356	100	0	0
		55	2.6	−0.241	88	0	12
		59	−18.1	−0.195	38	0	62
6	20.9	48	7.6	−0.317	100	0	0
		50	10.6	−0.289	100	0	0

[a]MAG calculations at the PBE/def2-TZVP/def2-SVP level; see Method Section for details.

in this work. For example, MO43 (Figure 4) of **5** has mainly Au 5d character (π-type) and gives positive contribution to

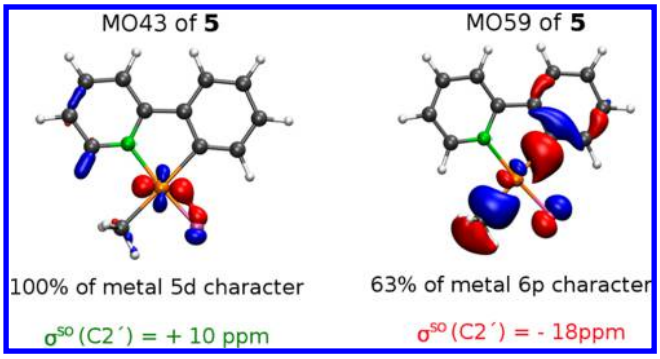

Figure 4. Visualization of two selected MOs of compound **5**, their contributions to the σ^{SO}(C2′) [note different signs of the σ^{SO}], and relative Au 6p and 5d AOs participation in the overall gold contribution to given MO.

σ^{SO}(C2′), whereas MO59 (Figure 4) of **5** mixes in the Au 6p character (σ-type) and gives a negative contribution to the σ^{SO}(C2′) in Table 2. Notably, such trends are observed for the whole series of the gold complexes **5**−**12**, see Table S2.

Analysis of MO → MO* magnetic couplings reveals that occupied σ^{SO}-active MOs with a large amount of the metal 5d character, found in platinum compounds (Figure 5, Tables S3−S4), typically couple with the lowest suitable vacant MOs, which have also a large amount of 5d character (5d → 5d* metal-based

DOI: 10.1021/ct501089z
J. Chem. Theory Comput. 2015, 11, 1509−1517

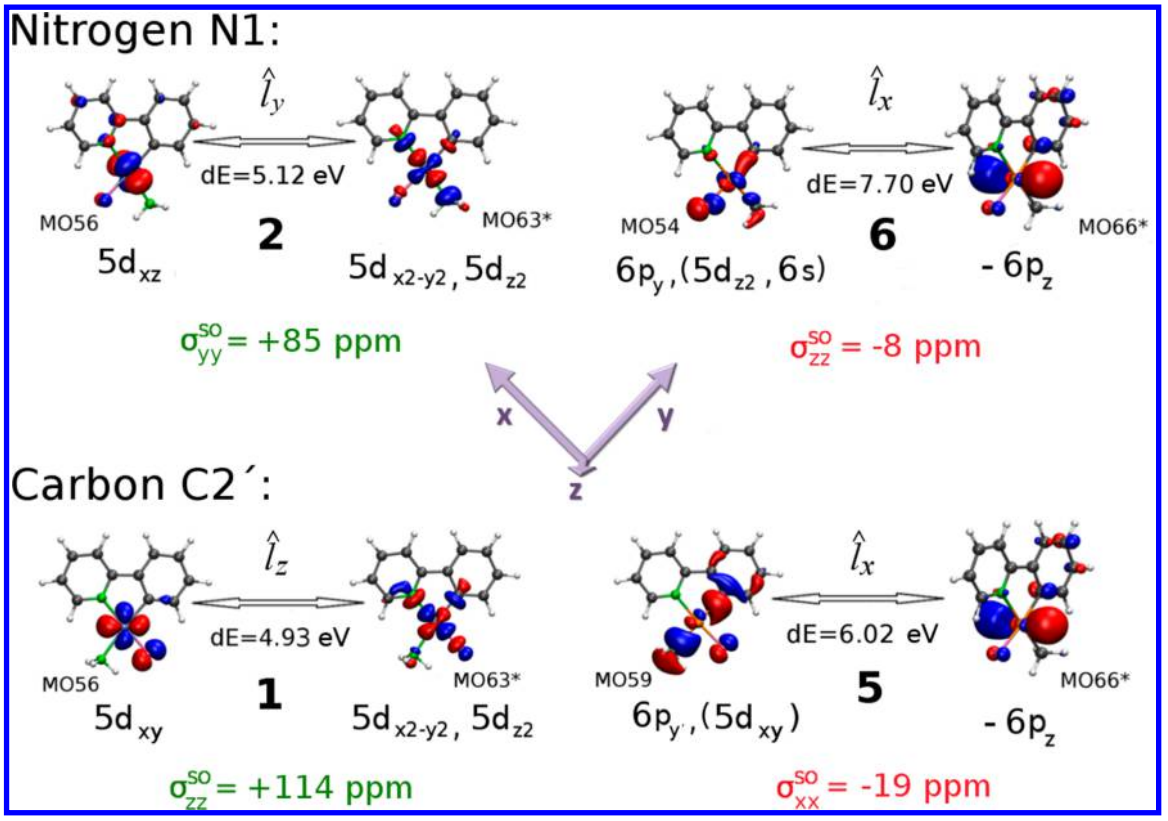

Figure 5. Selected MO → MO* magnetic couplings for **1** and **2** and for **5** and **6** in a coordinate system with *x* and *y* axes defined by the metal−ligand bonds, together with metal AO compositions of the corresponding MOs, contributions of given MO → MO* magnetic couplings to the particular principal components of the σ^{SO}(LA), and the energy differences between the occupied and vacant MOs. Generally, the principal axes of the SO shielding tensors do not coincide with the coordinate system axes displayed in this figure. They are shown in Figure 3.

magnetic couplings), see Figure 5 on the left. Small energy denominators (eq 1 and eq S1) combined with the high metal 5d character in both the occupied and vacant MOs make these efficient 5d → 5d* based magnetic couplings responsible for the large and positive σ^{SO}(LA) found in platinum complexes. We note that, in the SOS-DFPT approximation, the SO integrals included in the σ^{SO} in eq S1 will be nonzero only if corresponding occupied and virtual AOs have the same main and azimuthal quantum number, i.e., only 5d → 5d* based (and 6p → 6p* based) couplings will give nonzero contributions to σ^{SO}.

To provide a clear picture of this phenomenon, individual MO → MO* contributions to the principal components of σ^{SO} tensors (N1 and C2′) are analyzed and discussed in the following. Two examples of 5d → 5d* based magnetic couplings in platinum compounds with positive contributions to σ^{SO}(N1) and σ^{SO}(C2′) are shown in Figure 5 on the left. In compound **2**, the occupied MO56 is composed almost exclusively of Pt $5d_{xz}$ AO. Operator $\hat{l}_y$ couples $5d_{xz}$ with $5d_{z^2-x^2}$.[71,72] As the vacant MO63* is composed in our notation of $5d_{x^2-y^2}$ and $5d_{z^2}$, the MO56 → MO63* coupling induces SO shielding in σ^{SO}_{yy} component of N1 in **2** (Figure 5, top-left). Analogously, occupied MO56 in **1** is composed mainly of the Pt $5d_{xy}$ AO. Operator $\hat{l}_z$ couples $5d_{xy}$ with $5d_{x^2-y^2}$.[71,73] As the vacant MO63* in **1** is composed predominantly of $5d_{x^2-y^2}$, the MO56 → MO63* coupling induces shielding in the σ^{SO}_{zz} component of C2′ for **1** (see Figure 5, bottom-left). Both the above-mentioned magnetic couplings are responsible for a *shielding effect* (positive σ^{SO}).[71] In fact, a *pattern* can be revealed for the Pt complexes: The large shielding contributions to σ^{SO}(LA) arise predominantly from magnetic couplings of out-of-axis (π-type) Pt-based frontier orbitals with the lowest virtual orbitals, which are of on-axis type ($5d_{x^2-y^2}$, $5d_{z^2}$), see Figure 5, left.

The situation is strikingly different for the gold complexes **5** and **6** with significant Au 6s and 6p AO character and notably reduced Au 5d character of the σ^{SO}-active MOs, as compared to Pt compounds, Table S3. For example, occupied σ^{SO}-active MO54 of **6** mixes $6p_y$, $5d_{z^2}$, and 6s orbitals of Au, see top-right of Figure 5. The metal 6s orbital does not contribute directly to the SO effect, and contributions of atomic 5d orbitals in vacant MO66* required for the 5d → 5d* based magnetic couplings are vanishingly small. In contrast, vacant MO66* is composed predominantly of Au $6p_z$ AO, and therefore, the MO54 → MO66* magnetic coupling ($6p_y$ → $6p_z$* based) dominates the σ^{SO}_{zz} of N1 in compound **6** (Figure 5, top-right), which is oriented along the *x* axis of the molecular system (for orientations of principal axes, see Figure 3!). This magnetic coupling produces a deshielding (negative σ^{SO}) at N1. MO66* is the lowest virtual MO with considerable Au 6p character, while other vacant orbitals of suitable composition (significant gold 6p character) are notably higher in energy (∼LUMO+20 and higher, see Table S4). This is reflected in the size of the energy denominators (eq 1 and eq S1), leading to a number of relatively small contributions from particular MO → MO* magnetic couplings to σ^{SO}(N1) in compound **6**. The average energy denominator for the six most important MO → MO* magnetic couplings contributing to σ^{SO}(N1) in **6** is ∼15 eV, 3 times larger than the similar average in Pt compound **2** (∼5 eV), see Table S4. A similar pattern can be found for the SO shielding constant of C2′ in compound **5**, see Figure 5, bottom-right. The MO59 → MO66* magnetic coupling ($6p_y$ → $6p_z$* based) produces a deshielding of ca. −19 ppm in the

DOI: 10.1021/ct501089z
J. Chem. Theory Comput. 2015, 11, 1509−1517

σ^{SO}_{xx} principal component of the C2′ shielding tensor. Both 6p → 6p* based magnetic couplings discussed in this paragraph are responsible for the *deshielding effect* (negative σ^{SO}). Generally, the situation is more complicated in Au complexes (comparing to their Pt counterparts). There is a delicate balance of a number of small negative 6p → 6p* based and small positive 5d → 5d* based magnetic couplings.

3.3. Differences in the HA−LA (M−LA) Bonding between Pt^{II} and Au^{III} Complexes. The MO analysis of σ^{SO} in section 3.2 indicated that differences in σ^{SO}(LA) between Pt and Au complexes are related to the different AO compositions of σ^{SO}-active MOs. As the SO effects are propagated from the HA to LA through the HA−LA bond, the changes in σ^{SO}(LA) should be related to the different nature of metal−ligand bonding in Au and Pt complexes. This is not surprising. Conventionally, platinum is known as a standard 5d metal, while the chemical properties of gold are truly unique,[2,3] with the highest electron affinity of gold of all metals as an example.[74] This phenomenon is related to the relativistic contraction and stabilization, hence chemical activation of 6s and 6p orbitals in the gold atom, as described by Pyykkö and Desclaux in the 1970s.[75−77]

To illustrate qualitatively the differences between Pt and Au complexes, the frontier orbital energies of Pt^{2+} and Au^{3+} ions, calculated at three different levels of relativity treatment, are shown in Figure 6. The energies of frontier 5d, 6s, and 6p orbitals

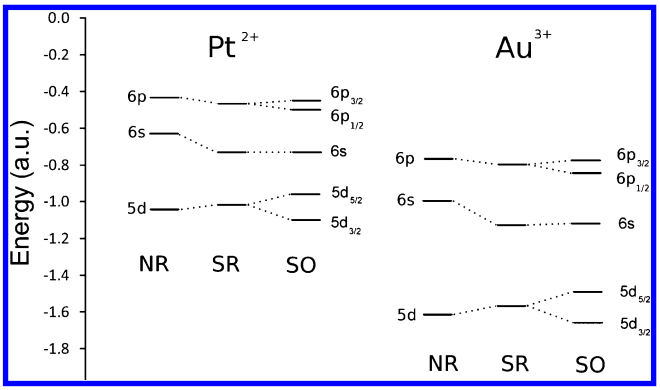

Figure 6. Calculated orbital energies of Pt^{2+} and Au^{3+} ions at nonrelativistic (NR), scalar-relativistic (SR), and scalar relativistic plus spin−orbit (SO) levels using the ZORA approach at the PBE-40/QZ4P level.

in Au^{3+} are significantly lower as compared to those in Pt^{2+} due to the larger nuclear charge of the Au nucleus and equal electron counts.[39] For both ions, the 6s and 6p orbitals are further stabilized in energy upon the inclusion of scalar relativity (SR-ZORA level), whereas the 5d orbitals are destabilized. Atomic orbitals 5d and 6p are further split by the spin−orbit coupling (SO-ZORA level). Due to a joint influence of the larger nuclear charge and the stronger SR effects, the 6s and 6p Au orbitals are situated energetically lower and can more easily participate in the bonding in Au complexes, whereas 5d orbitals are somewhat "deactivated" in the chemical bonding of gold. This is nicely reflected in the sign and size of σ^{SO} at the light ligand atom in gold complexes.

Generally, energies of occupied σ^{SO}-active MOs (discussed in section 3.2) in the series of Au complexes **5**−**12** are found lower than those in their Pt analogs **1**−**4** (Table 2). Differences in atomic orbital energies thus result in different bonding situations in Pt and Au complexes. To obtain a transparent account of the differences in the electronic structure of the Pt and Au complexes, comparative EHT calculations were performed, followed by the fragment molecular orbital (FMO) analysis of bonding between the metal ions and the ligands (Figures S3 and S4). Out of the many FMO interactions allowed by symmetry, only those whose contributions to metal−ligand Mulliken overlap population were at least 0.08 are considered below. On the basis of these criteria, there are four vacant fragment orbitals at the metal ion ($6p_x$, $6p_y$, 6s, and $5d_{x^2-y^2}$) which are mixing with occupied orbitals at the ligand for both Pt and Au complexes. On the ligand side, three fragment MOs are participating in all complexes.

In the case of platinum complexes **1** and **2**, all of the occupied MOs with significant contributions to the metal−ligand overlap population are at the central metal atom dominated by the Pt 5d orbitals (Table S5 and Figure S3 in the Supporting Information). This predominant 5d-type of bonding is related to the SO shielding at the LA ($+\sigma^{SO}$).

On the contrary, in the case of Au complex **5**, Au $5d_{x^2-y^2}$ AO contributes by more than 1% only to the lowest-lying MO in Figure S4a, while the other two occupied bonding MOs are formed by 6s and 6p metal orbitals. The bonding to C2′ is dominated by a metal $6p_y$ (not 5d) orbital, see MO36 in Figure S4a and its DFT-counterpart MO59 in Figures 4 and 5, hence the negative contribution to the σ^{SO}(C2′). Similarly to complex **5**, in complex **6** there is a significant contribution of the metal 6s and metal 6p AOs in the occupied bonding MOs (Table S5). In complex **6**, unlike **5**, the 6p orbitals dominate the Au−N bond, not the Au−C2′ bond (see Figure S4b). This is reflected in the negative σ^{SO}(N1), see Table 1. A DFT analysis of occupied MOs for compounds **1**−**12** (Table S6a and b) gives the results in accord with the EHT fragment analysis, i.e., stronger mixing of the metal 6s and 6p AOs into lower-lying MOs in Au compounds as compared to a stronger mixing of metal 5d AOs in Pt analogs.

3.4. Correlation of σ^{SO}(LA) with the Degree of Covalence of the HA−LA Bond. As demonstrated in the previous section, the σ^{SO}(LA) is related to the type of HA−LA bonding. It has been indicated previously that σ^{SO}(LA) is influenced by the ionicity or the covalence of the HA−LA bond.[39−41,43] However, to the best of our knowledge, the relationship between the covalence (the extent of electron sharing) and σ^{SO}(LA) has been characterized only qualitatively[39−41,78] with no demonstrated quantitative correlations.

The N1 and C2′ atoms of the 2ppy moiety (Figure 1) can be qualitatively regarded as two independent ligands: N1 as a neutral ligand which donates its free electron pair to the metal, and C2′ as a monoanion (with an overabundance of electrons). These differences between N1 and C2′ are reflected in their bonding to the central atom. The M−C2′ bond is short and more covalent than the M−N1 bond in all complexes **1**−**12** (Table S7). NBO analysis shows that the M−N1 bond is highly polarized, with an M/N1 AO ratio of ca. 15:85, while the M−C2′ bond is more covalent with an M/C2′ atomic orbital ratio of ca. 35:65.

The degree of covalence of any bond can be characterized by the delocalization index, DI, in the frame of Quantum Theory of Atoms in Molecules (QTAIM). Here, the delocalization index, δ(M↔LA), between M and LA (M = Pt, Au; LA = N1, C2′) is demonstrated to correlate with σ^{SO}(LA) (Table S8 and Figure S5). However, the DI for the M−C2′ is by about 30% larger than that for the M−N1 bond. Generally, the larger the difference in electronegativity of involved atoms, the smaller the DI for the bond they form. Accordingly, an ideal ionic bond has no electron sharing and DI = 0. Similarly, by increasing the difference in electronegativity between the two atoms, the covalent bond turns to a polar bond with lower DI. It is shown that the DI and

DOI: 10.1021/ct501089z
J. Chem. Theory Comput. 2015, 11, 1509−1517

σ^{SO}(LA) do correlate but with different intercepts for the different bonds (M−N1 vs M−C2′ in Figure S5). However, if DI is multiplied by the electronegativity of the light NMR spectator atom, all the lines merge; hence the DI × $\chi_{Pauling}$ function correlates generally with σ^{SO}(LA) for any M−LA pair considered here (Figure 7, Table S8). Clearly, the correlation between the

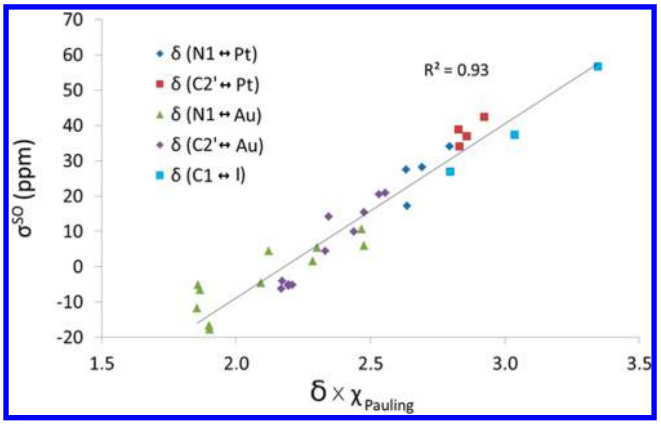

Figure 7. Correlation between the σ^{SO}(LA) and the delocalization index δ(M↔LA) multiplied by the electronegativity of the light NMR spectator atom ($\delta \times \chi_{Pauling}$) for the M−LA pair of atoms. The series includes platinum (nitrogen−blue rhomb, carbon−red square), gold (nitrogen−green triangle, carbon−violet rhomb), and iodine (carbon−blue square) compounds. For structures and values, see Figure S6 and Table S8.

σ^{SO}(LA) and the DI × $\chi_{Pauling}$ is retained not only for various types of light spectator atoms (^{13}C, ^{15}N) but even for different central metal atoms (Au, Pt) involved in the M−LA bonding (Figure 7), where the BDC concept[43] (cf. above) fails. To further demonstrate the versatility of this approach, the original set of 12 complexes was extended by additional Au and Pt complexes (Figure S6) as well as by several iodo-based compounds taken from ref 17. The Scaled HA−LA Delocalization INdex (SHALADIN), including the SO-coupling constant and electronegativity of the HA, is indicated to be a suitable candidate for describing the electronic-structure nature of changes in the σ^{SO}(LA). It is clear that this concept requires more extensive analysis and will be described in our forthcoming paper.

It should be noted that the covalence of the M−LA bond in each type of complex is altered by the *trans* effect, thoroughly discussed in our previous works on octahedral complexes.[42,43] As the *trans* ligand affects the character of the M−LA bond, it modulates the propagation of spin−orbit effects on the σ(LA) via the SO/FC mechanism. This modulation can be analyzed based on the energy denominators,[13] the s-character of the light atom[17] and the d-character of the metal[43] (or f-character for actinides)[79] in the M−LA bond, and the covalence of the M−LA bond as demonstrated in this paper.

4. CONCLUDING REMARKS

In the present work, the observed qualitative differences between the platinum and gold compounds in the magnitude and the sign of SO-induced nuclear magnetic shielding at the light atoms are related to the different nature of chemical bonding in Pt and Au systems and rationalized by the contraction of 6s and 6p atomic orbitals in Au complexes. The contraction is caused by the larger Au nuclear charge and the stronger scalar relativistic effects in gold complexes, resulting in a more efficient mixing of metal 6s and 6p AOs with ligand orbitals. This leads to significant 6s and 6p AOs contributions in the frontier MOs in Au compounds. Our quantitative DFT results are accompanied by a qualitative EHT analysis to simplify the underlying interactions in the systems.[80] The magnitude and the sign of the σ^{SO}(LA) can be understood on the basis of either a predominance of or a balance between various 5d → 5d* based and 6p → 6p* based orbital magnetic couplings contributing to the σ^{SO}. In the studied square-planar complexes, the former are typically large and positive and dominate the large shielding (positive σ^{SO}) in Pt complexes, whereas the latter are negative and lead to the small shielding or deshielding (negative σ^{SO}) in Au complexes.

Previously, different individual correlations of electronic structure effects with the SO-HALA nuclear magnetic (de)shielding have been described and discussed to provide simple and intuitive chemical understanding of the SO-induced NMR shielding. The concepts like the s-character of the LA in HA−LA bond, the d-character of the metal (HA) in HA−LA bond, the *trans* effect, and the effect of crystal field are all related to one mechanism. In present work, we demonstrate the correlation of the σ^{SO}(LA) with the degree of covalence of the M−LA bond. Indeed, the size of σ^{SO}(LA) is shown to correlate quantitatively with the electronegativity-scaled QTAIM delocalization index characterizing the M−LA bond. This new quantity is a candidate for a universal electronic-structure indicator of the size of SO-induced NMR shielding at the light atom. In parallel, the effect of the *trans* substituent on the σ^{SO}(LA) could be understood as a modification of the degree of covalence of the M−LA bonding via the *trans* effect. It is expected that the results and conclusions presented in this paper will contribute to understanding the relativistic effects on the experimental NMR parameters in heavy-element systems.

■ ASSOCIATED CONTENT

Supporting Information

Table S1: σ^{SO}(N1) and σ^{SO}(C2′) in compounds **1**−**12**. Figure S1: σ^{SO}(N1) vs Au d-character. Figure S2: σ^{SO}(C2′) vs Au d-character. Tables S2−S4: Detailed MO analyses of σ^{SO}(LA) for **1**−**12**. Figures S2.5, S3, S3.5, S3.7, S4, and S4.5: Composition of selected FMO and interaction FMO diagrams for compounds **1** and **2** (Pt) and **5** and **6** (Au). Table S5: Contributions of all metal AOs into occupied MOs plotted in Figures S3 and S4. Table S5.5: The contributions of selected metal FMOs to MOs in **1**, **2**, **5**, and **6**. Tables S6a and S6b: Lowest MOs with significant 6s and 6p metal AO contributions for **1**−**12**. Table S7: NBO analysis of M−N1 and M−C2′ bonds in compounds **1**−**12**. Figure S5: σ^{SO}(LA) vs δ(M↔LA). Figure S6: Structures of compounds **13**−**21** presented in the main text in Figure 7. Table S8: Electron delocalization indices and σ^{SO}(LA) for compounds **1**−**21**. This material is available free of charge via the Internet at http://pubs.acs.org.

■ AUTHOR INFORMATION

Corresponding Authors

*E-mail: straka@uochb.cas.cz.
*E-mail: radek.marek@ceitec.muni.cz.

Present Address

⊥Center for Molecular and Macromolecular Studies, Polish Academy of Sciences, Sienkiewicza 112, Łódź, Poland

Notes

The authors declare no competing financial interest.

DOI: 10.1021/ct501089z
J. Chem. Theory Comput. 2015, 11, 1509−1517

ACKNOWLEDGMENTS

This work was supported by the Czech Science Foundation (P206/12/0539 to J.V., M.L.M., M.S., and R.M.) and carried out at CEITEC − the Central European Institute of Technology with research infrastructure supported by the project CZ.1.05/1.1.00/02.0068 financed by the European Regional Development Fund. C.F.-N. thanks the Program "Employment of Newly Graduated Doctors of Science for Scientific Excellence" (Grant Number CZ.1.07/2.3.00/30.009) cofinanced by the European Social Fund and the state budget of the Czech Republic, and the SoMoPro II program (REA Grant Agreement No. 291782) cofinanced by the Seventh Framework Program of EU and the South-Moravian Region for financial support. The access to computing and storage facilities owned by parties and projects contributing to the National Grid Infrastructure MetaCentrum, and provided under the program "Projects of Large Infrastructure for Research, Development, and Innovations" (LM2010005), and the CERIT-SC computing and storage facilities, provided under the program Center CERIT Scientific Cloud, part of the Operational Program Research and Development for Innovations (CZ.1.05/3.2.00/08.0144), is acknowledged.

REFERENCES

(1) Pyykkö, P. *Chem. Rev.* **1988**, *88*, 563−594.
(2) Pyykkö, P. *Angew. Chem., Int. Ed.* **2004**, *43*, 4412−4456.
(3) Pyykkö, P. *Inorg. Chim. Acta* **2005**, *358*, 4113−4130.
(4) Kutzelnigg, W. In *Calculation of NMR and EPR Parameters*; Kaupp, M., Bühl, M., Malkin, V., Eds.; Wiley-VCH: 2004; pp 43−82.
(5) Autschbach, J. In High Resolution NMR Spectroscopy Understanding Molecules and Their Electronic Structures. *Science and Technology of Atomic, Molecular, Condensed Matter & Biological Systems*; Contreras, R. H., Ed.; Elsevier: 2013; Vol. 3, pp 69−117.
(6) Maldonado, A. F.; Aucar, G. A. *Phys. Chem. Chem. Phys.* **2009**, *11*, 5615−5627.
(7) Lantto, P.; Standara, S.; Riedel, S.; Vaara, J.; Straka, M. *Phys. Chem. Chem. Phys.* **2012**, *14*, 10944−10952.
(8) Kaupp, M. Relativistic Electronic Structure Theory Part 2. Applications. In *Theoretical and Computational Chemistry*; Schwerdtfeger, P., Ed.; Elsevier: 2004; Vol. Vol. *14*, pp 552−597.
(9) Vaara, J. *Phys. Chem. Chem. Phys.* **2007**, *9*, 5399−5418.
(10) Nakagawa, N.; Coelho, S.; Obinata, S. *6th NMR Symp.* **1967**, 8−8.
(11) Nomura, Y.; Takeuchi, Y.; Nakagawa, N. *Tetrahedron Lett.* **1969**, *10*, 639−642.
(12) Cheremisin, A. A.; Schastnev, P. V. *J. Magn. Reson.* **1969**, *40*, 459−468.
(13) Hegetschweiler, K.; Kuppert, D.; Huppert, J.; Straka, M.; Kaupp, M. *J. Am. Chem. Soc.* **2004**, *126*, 6728−6738.
(14) Pyykkö, P.; Görling, A. *Mol. Phys.* **1987**, *61*, 195−205.
(15) Autschbach, J. In *Calculation of NMR and EPR Parameters*; Kaupp, M., Bühl, M., Malkin, V., Eds.; Wiley-VCH Verlag GmbH: 2004; pp 227−247.
(16) Kaupp, M.; Malkin, O. L.; Malkin, V. G. *Chem. Phys. Lett.* **1997**, *265*, 55−59.
(17) Kaupp, M.; Malkina, O. L.; Malkin, V. G.; Pyykkö, P. *Chem.—Eur. J.* **1998**, *4*, 118−126.
(18) Malkina, O. L.; Schimmelpfennig, B.; Kaupp, M.; Hess, B. A.; Chandra, P.; Wahlgren, U.; Malkin, V. G. *Chem. Phys. Lett.* **1998**, *296*, 93−104.
(19) Kantola, A. M.; Lantto, P.; Vaara, J.; Jokisaari, J. *Phys. Chem. Chem. Phys.* **2010**, *12*, 2679−2692.
(20) Lantto, P.; Vaara, J. *J. Chem. Phys.* **2007**, *127*, 084312.
(21) Standara, S.; Maliňáková, K.; Marek, R.; Marek, J.; Hocek, M.; Vaara, J.; Straka, M. *Phys. Chem. Chem. Phys.* **2010**, *12*, 5126−5139.
(22) Nakatsuji, H.; Takashima, H.; Hada, M. *Chem. Phys. Lett.* **1995**, *233*, 95−101.
(23) Ballard, C. C.; Hada, M.; Kaneko, H.; Nakatsuji, H. *Chem. Phys. Lett.* **1996**, *254*, 170−178.
(24) Manninen, P.; Lantto, P.; Vaara, J.; Ruud, K. *J. Chem. Phys.* **2003**, *119*, 2623−2637.
(25) Vaara, J.; Manninen, P.; Lantto, P. In *Calculation of NMR and EPR Parameters*; Kaupp, M., Bühl, M., Malkin, V., Eds.; Wiley-VCH Verlag GmbH & Co. KGaA, 2004; pp 209−226.
(26) Manninen, P.; Ruud, K.; Lantto, P.; Vaara, J. *J. Chem. Phys.* **2005**, *122*, 114107.
(27) Manninen, P.; Ruud, K.; Lantto, P.; Vaara, J. *J. Chem. Phys.* **2006**, *124*, 149901(E).
(28) Rodriguez-Fortea, A.; Alemany, P.; Ziegler, T. *J. Phys. Chem. A* **1999**, *103*, 8288−8294.
(29) Roukala, J.; Maldonado, A. F.; Vaara, J.; Aucar, G. A.; Lantto, P. *Phys. Chem. Chem. Phys.* **2011**, *13*, 21016−21025.
(30) Melo, J. I.; Maldonado, A.; Aucar, G. A. *Theor. Chem. Acc.* **2011**, *129*, 483−494.
(31) Maldonado, A. F.; Gimenez, C. A.; Aucar, G. A. *Chem. Phys.* **2012**, *395*, 75−81.
(32) Maldonado, A. F.; Aucar, G. A.; Melo, J. I. *J. Mol. Model.* **2014**, *20*, 1−15.
(33) Vaara, J.; Ruud, K.; Vahtras, O.; Ågren, H.; Jokisaari, J. *J. Chem. Phys.* **1998**, *109*, 1212−1222.
(34) Vaara, J.; Ruud, K.; Vahtras, O. *J. Chem. Phys.* **1999**, *111*, 2900−2909.
(35) Dean, R. R.; Green, J. C. *J. Chem. Soc. A* **1968**, 3047−3050.
(36) Pidcock, A.; Richards, R. E.; Venanzi, L. M. *J. Chem. Soc. A* **1968**, 1970−1973.
(37) Wolff, S. K.; Ziegler, T. *J. Chem. Phys.* **1998**, *109*, 895−905.
(38) Hyvärinen, M.; Vaara, J.; Goldammer, A.; Kutzky, B.; Hegetschweiler, K.; Kaupp, M.; Straka, M. *J. Am. Chem. Soc.* **2009**, *131*, 11909−11918.
(39) Pawlak, T.; Munzarová, M. L.; Pazderski, L.; Marek, R. *J. Chem. Theory Comput.* **2011**, *7*, 3909−3923.
(40) Truflandier, L. A.; Brendler, E.; Wagler, J.; Autschbach, J. *Angew. Chem., Int. Ed.* **2011**, *50*, 255−259.
(41) Autschbach, J.; Sutter, K.; Truflandier, L. A.; Brendler, E.; Wagler, J. *Chem.—Eur. J.* **2012**, *18*, 12803−12813.
(42) Vícha, J.; Patzschke, M.; Marek, R. *Phys. Chem. Chem. Phys.* **2013**, *15*, 7740−7754.
(43) Vícha, J.; Straka, M.; Munzarová, M. L.; Marek, R. *J. Chem. Theory Comput.* **2014**, *10*, 1489−1499.
(44) Edwards, G. L.; Black, D. S. .; Deacon, G. B.; Wakelin, L. P. *Can. J. Chem.* **2005**, *83*, 969−979.
(45) Pawlak, T.; Niedzielska, D.; Vícha, J.; Marek, R.; Pazderski, L. *J. Organomet. Chem.* **2014**, *759*, 58−66.
(46) Parish, R. V.; Howe, B. P.; Wright, J. P.; Mack, J.; Pritchard, R. G.; Buckley, R. G.; Elsome, A. M.; Fricker, S. P. *Inorg. Chem.* **1996**, *35*, 1659−1666.
(47) Fan, D.; Yang, C.-T.; Ranford, J. D.; Lee, P. F.; Vittal, J. J. *Dalton Trans.* **2003**, 2680−2685.
(48) Adamo, C.; Barone, V. *J. Chem. Phys.* **1999**, *110*, 6158−6170.
(49) Weigend, F.; Ahlrichs, R. *Phys. Chem. Chem. Phys.* **2005**, *7*, 3297−3305.
(50) *TURBOMOLE*, V6.3 2011; University of Karlsruhe and Forschungszentrum Karlsruhe GmbH: 1989−2007; TURBOMOLE GmbH: 2007. Available from http://www.turbomole.com.
(51) Andrae, D.; Häußermann, U.; Dolg, M.; Stoll, H.; Preuß, H. *Theoret. Chim. Acta* **1990**, *77*, 123−141.
(52) Bühl, M.; Reimann, C.; Pantazis, D. A.; Bredow, T.; Neese, F. *J. Chem. Theory Comput.* **2008**, *4*, 1449−1459.
(53) Glendening, E. D.; Badenhoop, J. K.; Reed, A. E.; Carpenter, J. E.; Bohmann, J. A.; Morales, C. M.; Weinhold, F. *NBO 5.0*; Theoretical Chemistry Institute, University of Wisconsin: Madison, WI, 2001.
(54) Autschbach, J.; Zheng, S.; Schurko, R. W. *Concepts Magn. Reson.* **2010**, *36A*, 84−126.
(55) *SCM*; Theoretical Chemistry, Vrije Universiteit: Amsterdam, The Netherlands. http://www.scm.com.

DOI: 10.1021/ct501089z
J. Chem. Theory Comput. 2015, 11, 1509−1517

(56) Perdew, J. P.; Burke, K.; Ernzerhof, M. *Phys. Rev. Lett.* **1996**, *77*, 3865−3868.
(57) Perdew, J.; Burke, K.; Ernzerhof, M. *Phys. Rev. Lett.* **1997**, *78*, 1396.
(58) Keith, T. A.; Frisch, M. J. *J. Phys. Chem. A* **2011**, *115*, 12879−12894.
(59) Sadjadi, S.; Matta, C. F.; Lemke, K. H.; Hamilton, I. P. *J. Chem. Phys. A* **2011**, *115*, 13024−13035.
(60) Badri, Z.; Foroutan-Nejad, C.; Rashidi-Ranjbar, P. *Phys. Chem. Chem. Phys.* **2012**, *14*, 3471−3481.
(61) Keith, T. A. *AIMAll*, version 13.11.04; TK Gristmill Software: Overland Park, KS, 2014 (aim.tkgristmill.com).
(62) Cortés-Guzmán, F.; Bader, R. F. W. *Coord. Chem. Rev.* **2005**, *249*, 633−662.
(63) Foroutan-Nejad, C.; Shahbazian, S.; Marek, R. *Chem.—Eur. J.* **2014**, *20*, 10140−10152.
(64) Malkin, V. G.; Malkina, O. L.; Reviakine, R.; Arbuznikov, A. V.; Kaupp, M.; Schimmelpfennig, B.; Malkin, I.; Repiský, M.; Komorovský, S.; Hrobárik, P.; Malkin, E.; Helgaker, T.; Ruud, K.; *MAG- ReSpect*, version 2.1; Universität Würzburg; Würzburg, Germany, 2010.
(65) Hrobárik, P.; Hrobáriková, V.; Meier, F.; Repiský, M.; Komorovský, S.; Kaupp, M. *J. Phys. Chem. A* **2011**, *115*, 5654−5659.
(66) Frisch, M. J.; Trucks, G. W.; Schlegel, H. B.; Scuseria, G. E.; Robb, M. A.; Cheeseman, J. R.; Scalmani, G.; Barone, V.; Mennucci, B.; Petersson, G. A.; Nakatsuji, H.; Caricato, M.; Li, X.; Hratchian, H. P.; Izmaylov, A. F.; Bloino, J.; Zheng, G.; Sonnenberg, J. L.; Hada, M.; Ehara, M.; Toyota, K.; Fukuda, R.; Hasegawa, J.; Ishida, M.; Nakajima, T.; Honda, Y.; Kitao, O.; Nakai, H.; Vreven, T.; Montgomery, J. A., Jr.; Peralta, J. E.; Ogliaro, F.; Bearpark, M.; Heyd, J. J.; Brothers, E.; Kudin, K. N.; Staroverov, V. N.; Kobayashi, R.; Normand, J.; Raghavachari, K.; Rendell, A.; Burant, J. C.; Iyengar, S. S.; Tomasi, J.; Cossi, M.; Rega, N.; Millam, J. M.; Klene, M.; Knox, J. E.; Cross, J. B.; Bakken, V.; Adamo, C.; Jaramillo, J.; Gomperts, R.; Stratmann, R. E.; Yazyev, O.; Austin, A. J.; Cammi, R.; Pomelli, C.; Ochterski, J. W.; Martin, R. L.; Morokuma, K.; Zakrzewski, V. G.; Voth, G. A.; Salvador, P.; Dannenberg, J. J.; Dapprich, S.; Daniels, A. D.; Farkas, Ö.; Foresman, J. B.; Ortiz, J. V.; Cioslowski, J.; Fox, D. J. *Gaussian 09*; Gaussian Inc.: Wallingford, CT, 2009.
(67) Malkin, V. G.; Malkina, O. L.; Casida, M. E.; Salahub, D. R. *J. Am. Chem. Soc.* **1994**, *116*, 5898−5908.
(68) Vaara, J.; Malkina, O. L.; Stoll, H.; Malkin, V. G.; Kaupp, M. *J. Chem. Phys.* **2001**, *114*, 61−71.
(69) Te Velde, G.; Bickelhaupt, F. M.; Baerends, E. J.; Fonseca Guerra, C.; van Gisbergen, S. J. A.; Snijders, J. G.; Ziegler, T. *J. Comput. Chem.* **2001**, *22*, 931−967.
(70) Guerra, C. F.; Snijders, J. G.; te Velde, G.; Baerends, E. J. *Theor. Chem. Acc.* **1998**, *99*, 391−403.
(71) Mabbs, F. E.; Collison, D. *Electron Paramagnetic Resonance of d Transition Metal Compounds*; Elsevier: 2013.
(72) Autschbach, J.; Zheng, S. *Magn. Reson. Chem.* **2008**, *46*, S45−S55.
(73) Gilbert, T. M.; Ziegler, T. *J. Phys. Chem. A* **1999**, *103*, 7535−7543.
(74) Pyykkö, P. *Angew. Chem., Int. Ed.* **2002**, *41*, 3573−3578.
(75) Desclaux, J. P. *At. Data Nucl. Data Tables* **1973**, *12*, 311−406.
(76) Desclaux, J. P.; Pyykkö, P. *Chem. Phys. Lett.* **1976**, *39*, 300−303.
(77) Pyykkö, P.; Desclaux, J. P. *Acc. Chem. Res.* **1979**, *12*, 276−281.
(78) Sutter, K.; Autschbach, J. *J. Am. Chem. Soc.* **2012**, *134*, 13374−13385.
(79) Seaman, L. A.; Hrobárik, P.; Schettini, M. F.; Fortier, S.; Kaupp, M.; Hayton, T. W. *Angew. Chem., Int. Ed.* **2013**, *52*, 3259−3263.
(80) Munzarová, M. L.; Hoffmann, R. *J. Am. Chem. Soc.* **2002**, *124*, 4787−4795.

DOI: 10.1021/ct501089z
J. Chem. Theory Comput. 2015, 11, 1509−1517